

Monocular Depth Estimators: Vulnerabilities and Attacks

Alwyn Mathew*

Aditya Prakash Patra*

Jimson Mathew

Indian Institute of Technology Patna

{alwyn.pcs16, aditya.cs16, jimson}@iitp.ac.in

Abstract

Recent advancements of neural networks lead to reliable monocular depth estimation. Monocular depth estimation techniques have the upper hand over traditional depth estimation techniques as it only needs one image during inference. Depth estimation is one of the essential tasks in robotics, and monocular depth estimation has a wide variety of safety-critical applications like in self-driving cars and surgical devices. Thus, the robustness of such techniques is very crucial. It has been shown in recent works that these deep neural networks are highly vulnerable to adversarial samples for tasks like classification, detection and segmentation. These adversarial samples can completely ruin the output of the system, making their credibility in real-time deployment questionable. In this paper, we investigate the robustness of the most state-of-the-art monocular depth estimation networks against adversarial attacks. Our experiments show that tiny perturbations on an image that are invisible to the naked eye (perturbation attack) and corruption less than about 1% of an image (patch attack) can affect the depth estimation drastically. We introduce a novel deep feature annihilation loss that corrupts the hidden feature space representation forcing the decoder of the network to output poor depth maps. The white-box and black-box test compliments the effectiveness of the proposed attack. We also perform adversarial example transferability tests, mainly cross-data transferability.

Keywords: Monocular depth, Depth estimation, Adversarial attack

1 Introduction

Per-pixel depth estimation from more than one two-dimensional images is a well-explored research field in computer vision. Recently the surge in estimating per-pixel depth from a single two-dimensional image has increased in the research community. Monocular depth estimation poses a variety of real-world applications like autonomous driving, robot navigation, and surgical devices. Monocular depth estimation has been studied in numerous settings like supervised, semi-supervised, and self-supervised. The introduction of convolution neural network (CNN) for depth estimation has helped to gain significant improvement over other traditional

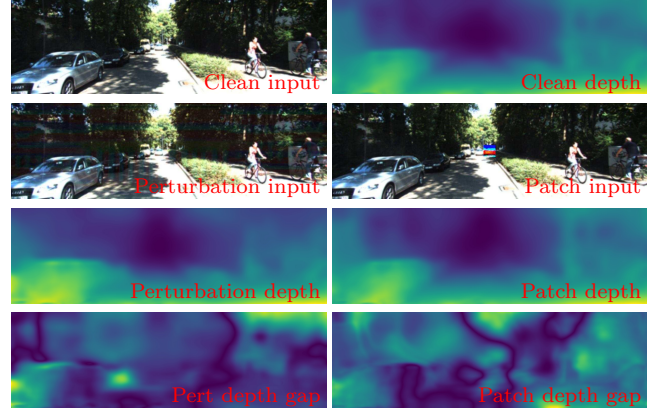


Figure 1: Adversarial attacks on monocular depth estimators. First row from left: Unattacked input image, Attacked input image with adversarial perturbation, Attacked input image with an adversarial patch. Second row from left: Depth estimated with SFM [32] with Unattacked input image, Attacked input image with adversarial perturbation, Attacked input image with an adversarial patch. Third row from left: Ground truth depth from LiDAR, Gap between unattacked depth and attacked depth with perturbation and patch attack.

methods. The supervised method considered monocular depth estimation as a regression problem with ground truth depth which are collected using devices like LiDAR and RGBD camera. However ground truth depth collection from these devices is a tedious task. The devices used for this purpose has its own downfalls. LiDAR produces a sparse depth map, and RGBD cameras have limitations on the maximum depth it can capture. The self-supervised method studies monocular depth estimation as a view synthesis problem using stereo images and/or video sequences. This view synthesis acts as the supervision of the system. The semi-supervised setting takes the best of both worlds by using sparse depth maps and multi view images for depth estimation.

Even though deep learning-based methods have shown astonishing results in most computer vision task, it has been shown that they are vulnerable to attacks. The vulnerability of deep learning models for tasks like image classification, detection, and segmentation is extensively studied in the literature. However, attacks on safety-critical models like depth estimation are not investigated broadly. In this paper, we investigate the robustness of monocular depth estimators

*Equal contribution.

against adversarial attacks. We mainly examine pixel perturbation and patch attack against a diverse set of depth estimators. There are few works on adversarial attacks on monocular depth estimation. But these attacks only focus on classical perturbation attacks like FGSM (Fast Gradient Sign Attack) and IFGSM (Iterative FGSM). FGSM is one of the most straightforward white-box adversarial attacks introduced in [10] which uses the gradient of the loss with respect to the input data, then adjusts the input data to maximize the loss. FGSM is a one-shot method, whereas IFGSM takes more than one gradient steps to find the perturbation. Some of the drawbacks of these attacks are:

1. Perturbation attacks like FGSM are image dependent and are not ideal for real-world attacks as it needs access to the image captured by the system to attack the model.
2. Defense against FGSM is more natural than adaptive perturbations generated by a network.

Existing adversarial attacks on classification, object detection, and segmentation aim to maximize non-essential softmax and minimize other softmax predictions of the network, thereby flipping the final prediction of the deep neural network. However, these attacks don't have a significant effect on the scene understanding models like depth estimation. Despite its success in basic vision tasks like classification, regression models can be attacked by these attacks to a very limited extent. In this work, we introduce a deep feature annihilation loss for both perturbation and patch attacks as shown in Figure 1. Deep feature annihilation (DFA) loss corrupts the internal representation of a deep neural network, rather than just the final layers. Attacks with DFA have demonstrated a more substantial effect on resultants. The main contributions of this paper are:

1. Show the vulnerability of monocular depth estimators against precisely calculated perturbation added to the input image.
2. Study the effect of patch attack on monocular depth estimators even when less than one percent of the image pixels are corrupted.
3. Introduce a novel Deep Feature Annihilation loss for stronger attacks.
4. Conducted extensive white and black-box testing for both perturbation and patch attack for monocular depth estimation.
5. Study the transferability of adversarial samples, mainly cross-model transferability and cross data transferability.

2 Related Works

2.1 Monocular Depth Estimation

Zhou *et al.*, [32] proposed an unsupervised depth estimation end-to-end framework from video sequence

where view synthesis act as the supervisory signal. Godard *et al.*, [8] estimate disparity from stereo images with a novel LR consistency loss. Mahjourian *et al.*, [19] introduced a 3D loss to enforce consistency of the estimated 3D point cloud. Yin *et al.*, [30] jointly learned monocular depth, optical flow and ego motion from videos in unsupervised manner. Luo *et al.*, [18] also jointly learned monocular depth, optical flow and ego motion from video but used these result to produce motion mask, occlusion mask, 3D motion map for rigid background and dynamic objects. Wang *et al.*, [28] proposed novel depth normalization strategy that substantially improves performance of the estimator. Godard *et al.*, [9] achieved state of the art results in KITTI rectified dataset with minimum reprojection loss, full-resolution multi-scale sampling and a mask that ignores training pixels that violate camera motion assumptions. Bian *et al.*, [3] proposes a scale consistent loss and a mask to handle moving and occluded objects. Lee *et al.*, [17] introduce a network architecture that utilizes novel local planer guidance layers to guide densely encoded features to estimate depth.

2.2 Adversarial Attack

In [27] Szegedy *et al.* shows that numerous state of the art neural networks are vulnerable to adversarial samples. Attacking a neural network with adversarial samples is called an adversarial attack. Adversarial attacks strive to make small perturbation in the network input so that it causes erroneous results. Attacks are mainly two types: perturbation attack and patch attack. The perturbation attack adds minute changes to pixels values so that its indistinguishable from the clean image but affects the prediction accuracy of the model. Patch attack adds a small patch that usually occupies less than one percent of the image and makes the result inaccurate. The drawback of the perturbation attack is that the attack needs to have access to the system to modify the image with the adversarial sample. Patch attacks succeed in this issue and can be placed at an apparent location in the scene to attack the model.

Goodfellow *et al.* [10] introduced a fast and straightforward perturbation attack called Fast Gradient Sign Attack (FGSM) that uses gradient with respect to input and adjust the input data to maximize the loss. Nguyen *et al.* [20] shows how easy it is to generate adversarial samples that are undetectable to the human eye. They have also shown completely unrecognizable attacked images classified with a high degree of confidence. Su *et al.* [25] reveals that even attacking a single pixel can change the classification prediction. [16] demonstrates a real physical adversarial attack in which a printed adversarial example can also affect the prediction correctness. [1] reflects the existence of 3D adversarial samples, which can fool classification models in different viewpoints, transformations, and cameras. [23] fooled facial recognition system with adversarial glasses and [6] ticked stop sign classifier by placing adversarial stickers over it.

2.3 Adversarial Attack on Scene Understanding

Adversarial attacks in tasks like detection, semantic segmentation, and reinforcement learning are studied in [2, 11, 29]. We mainly focus on attacks toward scene understanding tasks like depth estimation. Ranjan *et al.* [22], shows the effect of adversarial patch attack on optical flow estimation. They have demonstrated that corrupting less than one percent of the pixels with a patch can deteriorate the prediction quality. The effect of adversarial patch extends beyond the region of the attack in some of the optical flow estimation models. In essence, the encoder-decoder architecture based models found to be more sensitive than spatial pyramid architecture. They also visualized feature maps of successful and failed attacks to understand the essence under the hood. Hu *et al.* [12] studies basic perturbation attacks like IFGSM (Iterative FGSM) on monocular depth estimation and also proposes a defense mechanism based on [13]. The perturbations non-salient parts are marked out to defend against the attack. Zhang *et al.* [31] explores basic perturbation attacks with FGSM, IFGSM, and MI-FGSM (Momentum IFGSM) for non-targeted, targeted, and universal attack in monocular depth estimation. In contrast, we investigate global and image dependent perturbation with a novel DFA loss that attacks deep feature maps rather than final activation like [12] and [31]. We also conducted an extensive study adversarial patch attacks on monocular depth estimators, which are more significant in a real-world attack. The transferability of both global perturbation and patch are studied in this work.

3 Approach

The robustness of a model that predicts depth from one or more images is considered to be a safety-critical task. We aim to optimize pixel intensity change in an image so that it affects the final prediction of the depth estimation models. These pixel intensity changes can occur in mainly two ways:

1. Adding a small perturbation to the clean image in a way that it's indistinguishable from the clean image as briefed in Section 3.1.
2. Corrupting few pixels, usually less than 1% in the image as briefed in Section 3.2.

Say $D \in \mathbb{R}^{h \times w}$ where $D(x, y)$ is the ground truth depth value at pixel location (x, y) where $x \in \mathbb{Z}_+^h, y \in \mathbb{Z}_+^w$ of a clean image $I \in \mathbb{R}^{h \times w \times 3}$, the attacked adversarial image $\tilde{I} \in \mathbb{R}^{h \times w \times 3}$ will force the model to predict a wrong estimate $\tilde{D} \in \mathbb{R}^{h \times w}$ with a constraint that $I(x, y) \approx \tilde{I}(x, y)$ and h, w is the height and width of the image. Though an adversarial sample can be created against the objective by maximizing the loss between predicted and ground-truth value, but ground truth depth maps are scarce. Widely popular autonomous dataset like KITTI [7] provides sparse LiDAR ground

truth but are very limited in number. The indoor NYU dataset [24] consists of dense depth ground truth, but the depth range are limited to the RGBD camera.

Ground truth data collected from devices like Sonar, Radar, and Lidar can be used to train a supervised depth estimation model. But supervised depth learning requires a vast amount of ground truth depth data, and these depth sensors have their error and noise characteristics, which will affect the learning process of the deep neural network. 3D lasers depth sensors measurements are typically much sparser than the image and thus lack detailed depth inference. These sensors also require accurate calibration and synchronization with the cameras. Rather than relying on ground truth depth information, an alternative approach to train a model to estimate depth is by self-supervised fashion using stereo image pairs and/or video streams from a single camera. The self-supervision signal comes from the loss between the synthesized view and the target view. View synthesis is another extensively explored problem in computer vision, where the objective is to reconstruct a specific view from one or more given views.

As all state of the art approaches are self-supervised, in this investigation we study five self-supervised monocular depth estimators, namely, SFM (Structure from motion) [32], SCSFM (Scale-Consistent SFM) [3], Monodepth1 [8], DDVO (Direct Depth Visual Odometry) [28], Monodepth1 [8], Monodepth2 [9], and B2F [14]. SFM, SCSFM, DDVO, B2F and Monodepth2 learns depth from monocular video but Monodepth1 uses stereo images. Monodepth2 also extends there work to stereo and stereo + videos training. Due to the limited availability of ground truth data, the depth network prediction of the clean image is taken as pseudo ground truth. Using these pseudo ground truths for attack makes it easy to attack a model in the absence of actual ground truth.

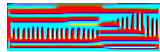
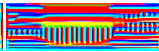
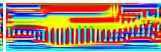
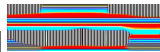
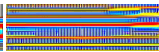
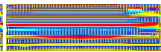
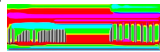
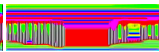
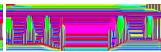


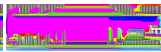
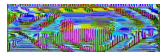
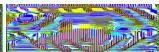
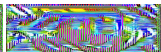
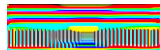
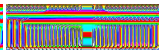
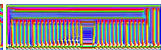
Models	Perturbation constrain		
	$\eta = 0.01$	$\eta = 0.05$	$\eta = 0.1$
SFM [32]			
DDVO [28]			
B2F [14]			
SCSFM [3]			
Mono1 [8]			
Mono2 [9]			

Figure 2: Adversarial perturbation generated to attack each models under different η .

3.1 Perturbation Attack

A depth network M that estimates depth D from a single image $I \in \mathbb{R}^{h \times w \times 3}$ as shown in Equ. 1, is at-

tacked by adding a perturbation $\alpha \in \mathbb{R}^{h \times w}$ to I as shown in Equ. 3. The perturbation α is constrained with η when added to an image to make the added perturbation unapparent to the naked eye as shown in Equ. 2. The perturbation is designed to be undetected in the attacked image \tilde{I} , and the attacked image looks as close as possible to the clean image I . The response of the network M at attacked image \tilde{I} is \tilde{D} .

$$D = M(I) \quad (1)$$

$$\tilde{I} = Adv(I, \alpha, \eta) = I + \eta * \alpha \quad (2)$$

$$\tilde{D} = M(Adv(I, \alpha, \eta)) \quad (3)$$

We basically experiment with two forms of perturbation namely global α_G and image-specific α_I perturbation. A perturbation network P is used to generate image-specific or global perturbation. P is a trivial encoder-decoder architecture based deep neural network. The image-specific perturbation network is trained with an unattacked image as input like $\alpha_I = P(I)$. This perturbation needs access to the input image to generate a perturbation noise which makes it less suitable for real-world attack (qualitative analysis in Supplementary material). However the global perturbation network is trained with random noise as input like $\alpha_G = P(\mathcal{N})$ where $\mathcal{N} \sim \mathcal{U}(0, 1) \in \mathbb{R}^{h \times w}$. This perturbation has a higher chance of attacking a system in real world as compared to image-specific perturbation, thus in this investigation we focus on global perturbation. Both image-specific and global perturbation are optimized by minimizing DFA loss (see Section 3.3). The optimized global perturbations for monocular depth estimators with different η is shown in Figure 2.

3.2 Patch Attack

A depth network M which estimates depth D from a single image $I \in \mathbb{R}^{h \times w \times 3}$ is attacked by placing an adversarial patch $\beta \in \mathbb{R}^{H \times W}$ on the image I at location ξ as shown in Equ. 4 where H, W is less than 1% of image size h, w . Transformations ω includes rotation and scaling are applied on the patch β randomly to make the patch invariant to these transformations. The response of the network M at attacked image $Adv(I, \beta, \omega, \xi)$ is \tilde{D} .

$$\tilde{D} = M(Adv(I, \beta, \omega, \xi)) \quad (4)$$

Adversarial patches are generated by optimizing random noise initialized with $\mathcal{N} \sim \mathcal{U}(0, 1) \in \mathbb{R}^{H \times W}$ by a neural network. The optimization minimizes DFA (see Section 3.3) to create global patches that are apt for real-world attacks. The square patches we optimized for monocular depth estimators are of different sizes i.e., 50×50 , 60×60 , 72×72 and 100×100 which are approximately 0.5%, 0.75%, 1% and 2% of the original KITTI image size 1242×375 as shown in Figure 3.

3.3 Deep Feature Annihilation loss

As compared to networks for tasks like classification and detection, regression networks are much more dif-


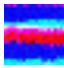
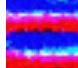
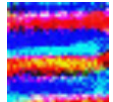


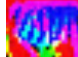

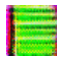


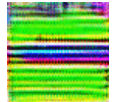

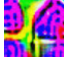
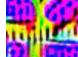




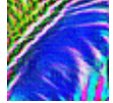




Models	Patch size			
	50×50	60×60	72×72	100×100
SFM [32]				
DDVO [28]				
B2F [14]				
SCSFM [3]				
Mono1 [8]				
Mono2 [9]				

Figure 3: Adversarial patches of different sizes optimized to attack each models.

ficult to attack, especially depth estimation networks. To deal with this issue, we introduce a novel DFA loss L_{dfa} , which attacks the internal feature representation of the input image. Note that we are optimizing the following objective after every convolution layer sparing few initial encoder layers.

$$F_l = F_l^{att} \times F_l^{org} \quad (5)$$

$$L_{dfa} = \sum_l \log[1 + \mathbb{E}(F_l^2) - \mathbb{E}(F_l)^2] W_l \quad (6)$$

The aim is to minimize the variance of correlation between the features maps F_l^{org} and F_l^{att} where F_l^{org}, F_l^{att} are the activations obtained from layer l in the depth network M after passing the unattacked image and attacked image through the network, respectively weighted with an empirically found W_l . This objective forces non-dominant activation values to increase while forcing the dominant activation values to decrease, resulting in the reduction of variance as shown in Figure 9. Variance reduction ends up costing network much semantic information, which makes the decoder incompetent to propagate useful information to output proper depth map. We have experimented by limiting the loss to just a variance reduction of F_l^{att} ; however, our objective of minimizing the variance of correlations works much better in practice.

4 Experiments

Adversarial attacks can be categorized mainly in two ways: the desired perturbation type and assumption

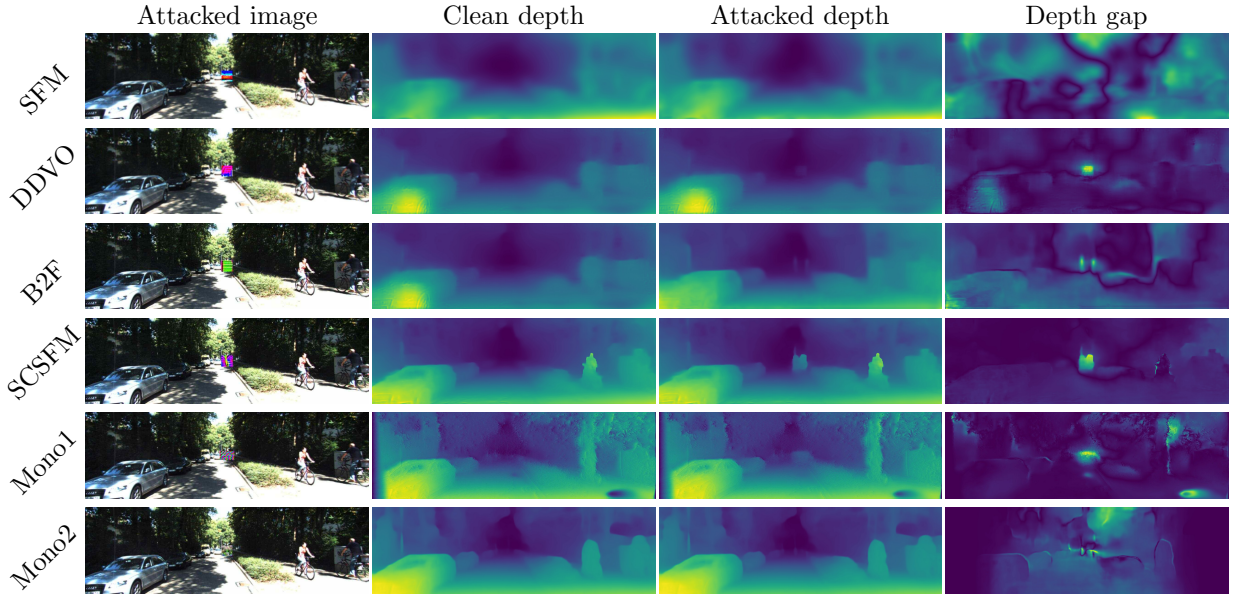


Figure 4: White-box patch test with patch size 50×50 .

Methods	Clean RMSE	Attacked							
		50×50		60×60		72×72		100×100	
		RMSE	Rel (%)	RMSE	Rel (%)	RMSE	Rel (%)	RMSE	Rel (%)
SFM [32]	6.1711	6.6232	8	7.844	28	8.8061	43	9.2719	51
DDVO [28]	5.5072	5.963	9	6.3477	16	6.9496	27	7.5986	45
B2F [14]	5.1615	5.5533	8	5.7199	11	6.1145	18	6.6022	28
SCSFM [3]	5.2271	6.4036	23	6.7562	30	7.1606	37	8.0283	54
Mono1 [8]	5.1973	5.7658	11	6.0623	17	6.2326	20	7.1151	37
Mono2 [9]	4.9099	5.3133	9	5.4127	11	5.5343	13	6.1714	26

Table 1: White-box patch attack at different patch sizes. Root mean square error (RMSE) of each model with and without adversarial attack and relative degradation (Rel) of RMSE on KITTI 2015.

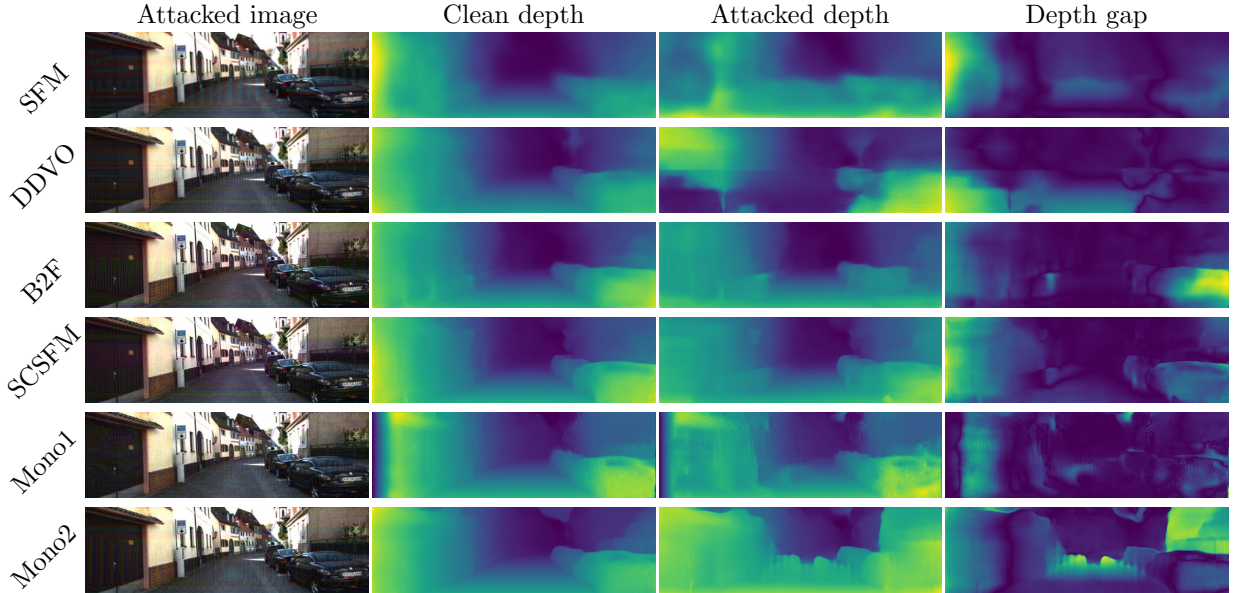


Figure 5: White-box perturbation test when $\eta = 0.05$.

of the attacker’s knowledge. Two perturbation types used in this investigation are briefed in Section 3.1 and Section 3.2. In this section, the kinds of assumptions of the attacker’s knowledge will be discussed, particularly, white-box and black-box attack.

4.1 White-box Attack

In a white-box attack, the attacker has full knowledge and access to the target model, including network architecture, input, output, and weights. We op-

Methods	Clean RMSE	Attacked					
		$\eta = 0.01$		$\eta = 0.05$		$\eta = 0.1$	
		RMSE	Rel (%)	RMSE	Rel (%)	RMSE	Rel (%)
SFM [32]	6.1711	6.2619	2	8.2988	35	10.1711	75
DDVO [28]	5.5072	5.6649	3	10.9875	100	18.3904	234
B2F [14]	5.1615	5.2876	3	6.7341	31	10.2199	99
SCSFM [3]	5.2271	5.277	1	6.5294	25	9.8324	89
Mono1 [8]	5.1973	5.2217	1	6.8002	31	12.0708	133
Mono2 [9]	4.9099	4.9984	2	9.8473	101	13.5497	176

Table 2: White-box perturbation attack at different perturbation constrains η .

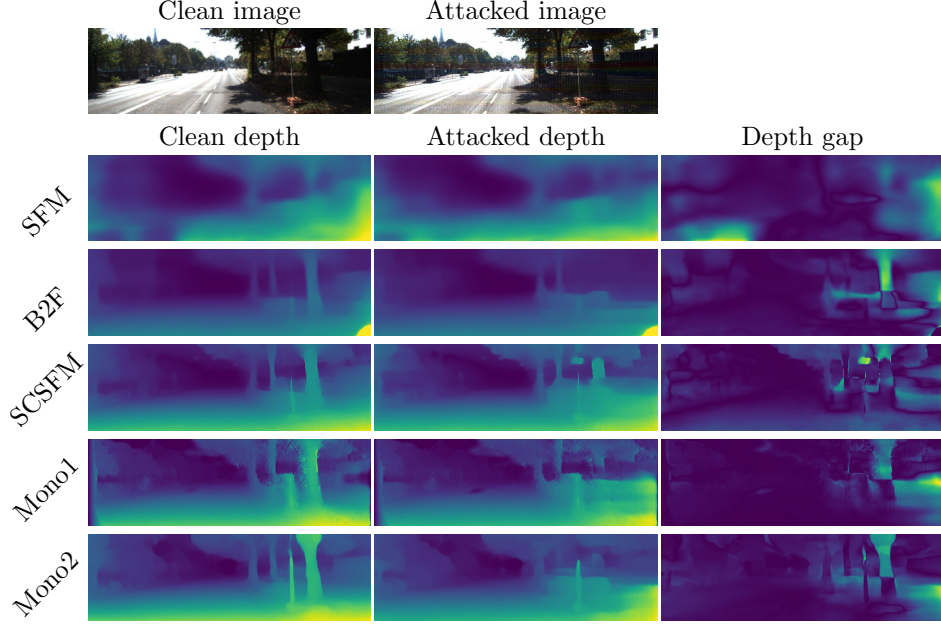


Figure 6: Black box perturbation test with $\eta = 0.05$.

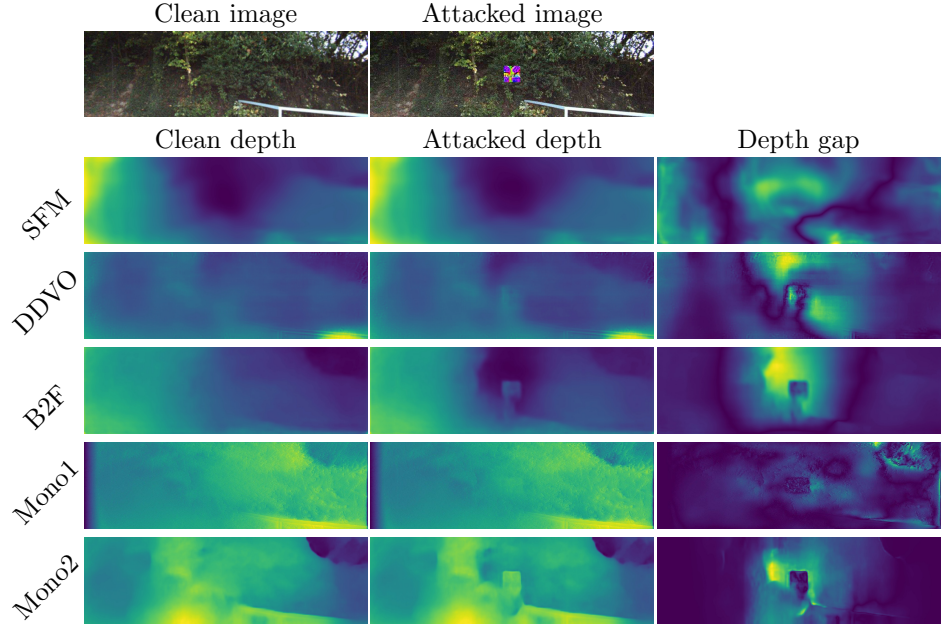


Figure 7: Black box for adversarial patch of size 72×72 .

timized adversarial samples in both perturbation and patch type. Generated perturbation is the same size as the input image of the target model. The perturba-

tion was optimized in such a way that it is imperceivable to our naked eye. The perturbation added to the input image is constrained in our experiments in the

Methods	Perturbation											
	SFM [32]		DDVO [28]		B2F [14]		SCSFM [3]		Mono1 [8]		Mono2 [9]	
	RMSE	Rel (%)	RMSE	Rel (%)	RMSE	Rel (%)	RMSE	Rel (%)	RMSE	Rel (%)	RMSE	Rel (%)
SFM [32]	-	-	6.818	11	6.3894	4	6.2981	3	6.2668	2	6.5082	6
DDVO [28]	6.3922	17	-	-	6.1185	12	5.7431	5	5.7929	6	6.0563	10
B2F [14]	5.8541	14	5.9961	17	-	-	6.0593	18	5.5322	8	5.772	12
SCSFM [3]	5.6802	9	5.7216	10	5.9632	15	-	-	5.4092	4	5.6468	9
Mono1 [8]	5.2791	2	5.5388	7	5.4201	5	5.4602	6	-	-	5.4485	5
Mono2 [9]	5.7929	18	5.7408	17	5.526	13	5.6306	15	5.2432	7	-	-

Table 3: Black-box perturbation attack when $\eta = 0.05$.

Methods	Clean	Patch									
		SFM [32]		DDVO [28]		SCSFM [3]		Mono1 [8]		Mono2 [9]	
		RMSE	Rel (%)	RMSE	Rel (%)	RMSE	Rel (%)	RMSE	Rel (%)	RMSE	Rel (%)
SFM [32]	6.1711	-	-	7.5362	23	6.3677	4	6.7395	10	6.2181	1
DDVO [28]	5.5072	5.9095	8	-	-	5.6998	4	5.7942	6	5.5974	2
B2F [14]	5.1615	5.7002	11	5.6992	11	5.6442	10	5.5763	9	5.374	5
SCSFM [3]	5.2271	6.599	27	6.5846	26	-	-	6.5564	26	5.2272	0
Mono1 [8]	5.1973	6.1638	19	5.9163	14	5.8969	14	-	-	5.5173	3
Mono2 [9]	4.9099	5.4502	12	5.4289	11	5.4155	11	5.5037	13	-	-

Table 4: Black-box attack for adversarial patch of size 72×72 .

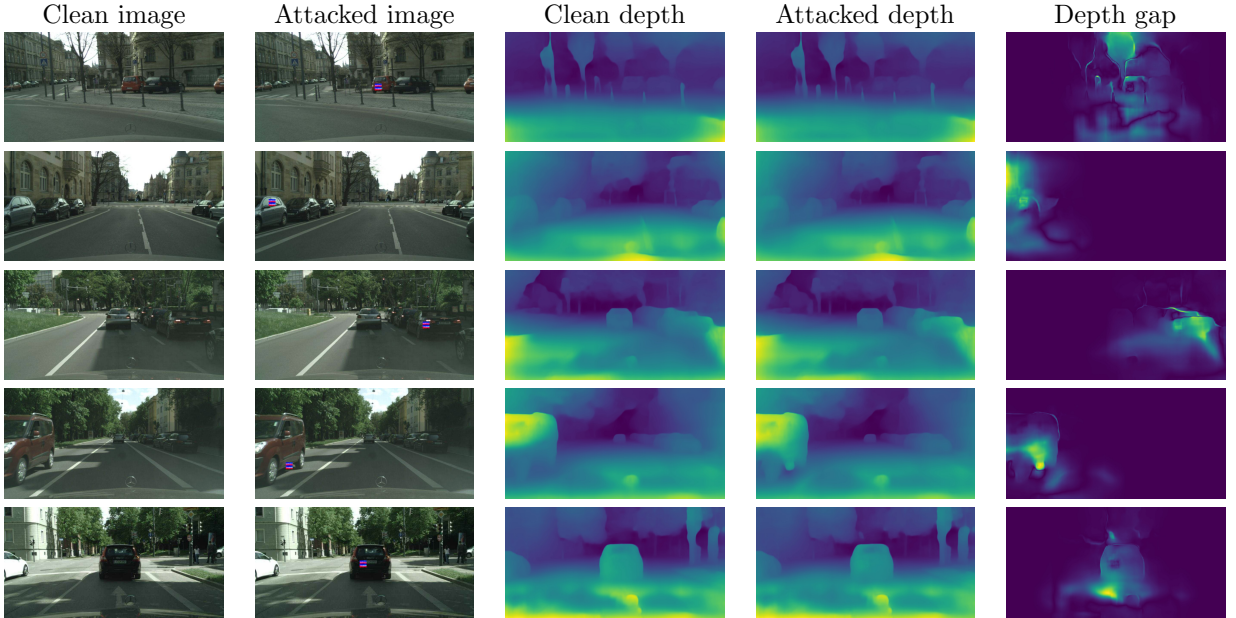


Figure 8: Cross-data transferability. KITTI [7] dataset adversarial patch used to attack images from Cityscape [4] dataset.

range of $[0.01, 0.1]$ as shown in Figure 14 and Table 2. For patch type attack we generate square adversarial patches on each network independently. All patches estimated for these networks are global, i.e., doesn't depend on the image where it is pasted. Each patch is augmented to make it invariant to rotation and location. Rotation is sampled randomly from $n \times \frac{\pi}{2}$ where $n \in \mathbb{Z}_+ : 0 \leq n \leq 4$ and location from $\xi(x, y)$ where $(x, y) \in \mathbb{Z}_+ : 0 \leq x \leq w, 0 \leq y \leq h$. The patch and perturbation are optimized with 45000+ image frames from the KITTI dataset. The output from the respective pretrained model in response to the clean image is treated as pseudo ground truth to optimize the adversarial sample. Then the DFA loss between network's responses from a clean image and an attacked image is minimized. Stochastic Gradient Descent (SDG) [26] with learning rate 0.01 and Adam [15] with learning rate 0.001, $\beta_1 = 0.9$, $\beta_2 = 0.999$ are used to optimize

perturbation and patch, respectively, in PyTorch [21].

4.2 Black-box Attack

In a black-box attack, the attacker has access to input and output but not to target network architecture and weights. The black-box attack is the most realistic attack, especially in safety-critical applications. These applications are designed in such a way that the attacker doesn't have direct access to the system. A global perturbation and patch learned from different models in the investigation are used for this attack. The global adversarial sample is optimized like a white-box attack. Even though adversarial samples are successful in attacking deep learning models with small perturbation or by corrupting few pixels, the transferability property of the adversarial samples makes it a severe threat. It has been shown that adversarial sam-

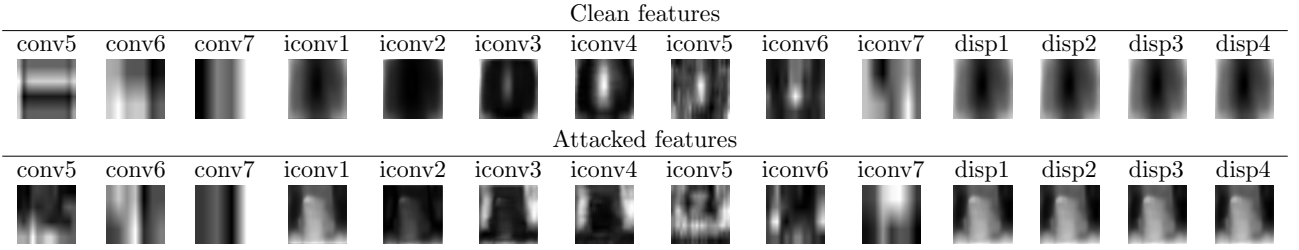


Figure 9: Layer-wise SFM [32] feature visualization. ‘convx’ are encoder layers and ‘iconvx’ are decoder layers.

ples are cross-model transferable i.e., adversarial perturbation optimized to attack Model A can be used to attack Model B which deals with the same task. Let Model A be an open-sourced model trained to estimate per-pixel depth from an image, with the transferability property; an attacker can attack a closed Model B effectively using Model A’s adversarial samples. In this study, we analyzed the transferability of the adversarial sample across all models under investigation. We also study cross-data transferability of the learned patch as shown in Figure 8. Cross-data transferability examines how well an adversarial sampled can be optimized with a publicly available dataset A to attack a model on proprietary data. The adversarial patch learned from KITTI dataset was used to attack images from Cityscape [4], considering KITTI as open source data and cityscape as proprietary data. This transferability assures that publicly available data can be used to attack almost any related models.

4.3 Evaluation

The qualitative evaluation of the attacks are conducted using metrics in [5] with KITTI 2015 dataset [7]. Root mean square error (RMSE) along with relative degradation (Rel) of RMSE are used to measure the vulnerability of the depth networks (Absolute relative error metric in supplementary material). As shown in Table 1 and Table 2, its evident that all state-of-the-art models are vulnerable to adversarial samples in white-box attacks. Our adversarial perturbation could attack all models very well and in few networks like DDVO and Mono2 just 5% of corruption could cause more than 100% damage to the depth maps. We can also see that corrupting less than even 1% of the image using the adversarial patch can cause more than 20% damage in the estimated depth map and also the damage extends significantly beyond the region of the patch thus making it a very dangerous real world attack. The qualitative result in Table 3 and Table 4 assure successful black-box attack on all state-of-the-art monocular depth estimation networks.

4.4 Analyze Deep Features

Unlike most adversarial attacks, in this investigation, we corrupt the network’s internal representation of an input image with our perturbation. In our experiment, striking the final layer alone didn’t affect the prediction drastically for monocular depth estimation. The ad-

versarial samples generated from existing methods still preserve a high level of input information in its deep hidden layers. These extracted features obstruct the desired attack in the model. To counter this issue, we targeted deep features representation of the input image to generate adversarial noise. We visualized deep features of attacked and clean image in Figure 9. For better visualization, feature outputs of zero image are taken as a clean image, and perturbation added to zero image is considered as an attacked image. It shows how each network layer reacts to the clean image and how the decoder layers react to an attacked image and exhibit an activation inversion property. From the visualization we can see that suppressed and non-dominant activations are exaggerated while dominant activations are weakened thus justifying our earlier claim. DFA makes the internal feature representation hollow and thereby creating a more robust attack on the final prediction of the network.

5 Conclusion

In this paper, we proposed an effective adversarial attack on monocular depth estimators. We explored both perturbation and patch type attacks in this study. The adversarial samples are designed with DFA loss to destroy the internal representation of the network, thereby resulting in a more vigorous attack. The attacks are evaluated extensively with white-box and black-box testing on KITTI dataset. The deep features of the network are visualized for a better understanding of the proposed attack. Also, cross-data transferability of the attack is examined.

References

- [1] Anish Athalye, Logan Engstrom, Andrew Ilyas, and Kevin Kwok. Synthesizing robust adversarial examples. *arXiv preprint arXiv:1707.07397*, 2017.
- [2] Vahid Behzadan and Arslan Munir. Vulnerability of deep reinforcement learning to policy induction attacks. In *International Conference on Machine Learning and Data Mining in Pattern Recognition*, pages 262–275. Springer, 2017.
- [3] Jiawang Bian, Zhichao Li, Naiyan Wang, Huangying Zhan, Chunhua Shen, Ming-Ming Cheng, and Ian Reid. Unsupervised scale-consistent depth and

- ego-motion learning from monocular video. In *Advances in Neural Information Processing Systems*, pages 35–45, 2019.
- [4] Marius Cordts, Mohamed Omran, Sebastian Ramos, Timo Rehfeld, Markus Enzweiler, Rodrigo Benenson, Uwe Franke, Stefan Roth, and Bernt Schiele. The cityscapes dataset for semantic urban scene understanding. In *Proceedings of the IEEE conference on computer vision and pattern recognition*, pages 3213–3223, 2016.
 - [5] David Eigen, Christian Puhersch, and Rob Fergus. Depth map prediction from a single image using a multi-scale deep network. In *Advances in neural information processing systems*, pages 2366–2374, 2014.
 - [6] Ivan Evtimov, Kevin Eykholt, Earlene Fernandes, Tadayoshi Kohno, Bo Li, Atul Prakash, Amir Rahmati, and Dawn Song. Robust physical-world attacks on deep learning models. *arXiv preprint arXiv:1707.08945*, 2017.
 - [7] Andreas Geiger, Philip Lenz, Christoph Stiller, and Raquel Urtasun. Vision meets robotics: The kitti dataset. *The International Journal of Robotics Research*, 32(11):1231–1237, 2013.
 - [8] Clément Godard, Oisín Mac Aodha, and Gabriel J Brostow. Unsupervised monocular depth estimation with left-right consistency. In *Proceedings of the IEEE Conference on Computer Vision and Pattern Recognition*, pages 270–279, 2017.
 - [9] Clément Godard, Oisín Mac Aodha, Michael Firman, and Gabriel J Brostow. Digging into self-supervised monocular depth estimation. In *Proceedings of the IEEE International Conference on Computer Vision*, pages 3828–3838, 2019.
 - [10] Ian J Goodfellow, Jonathon Shlens, and Christian Szegedy. Explaining and harnessing adversarial examples. *arXiv preprint arXiv:1412.6572*, 2014.
 - [11] Jan Hendrik Metzen, Mummadi Chaithanya Kumar, Thomas Brox, and Volker Fischer. Universal adversarial perturbations against semantic image segmentation. In *Proceedings of the IEEE International Conference on Computer Vision*, pages 2755–2764, 2017.
 - [12] Junjie Hu and Takayuki Okatani. Analysis of deep networks for monocular depth estimation through adversarial attacks with proposal of a defense method. *arXiv preprint arXiv:1911.08790*, 2019.
 - [13] Junjie Hu, Yan Zhang, and Takayuki Okatani. Visualization of convolutional neural networks for monocular depth estimation. In *Proceedings of the IEEE International Conference on Computer Vision*, pages 3869–3878, 2019.
 - [14] Joel Janai, Fatma Guney, Anurag Ranjan, Michael Black, and Andreas Geiger. Unsupervised learning of multi-frame optical flow with occlusions. In *Proceedings of the European Conference on Computer Vision (ECCV)*, pages 690–706, 2018.
 - [15] Diederik P Kingma and Jimmy Ba. Adam: A method for stochastic optimization. *arXiv preprint arXiv:1412.6980*, 2014.
 - [16] Alexey Kurakin, Ian Goodfellow, and Samy Bengio. Adversarial examples in the physical world. *arXiv preprint arXiv:1607.02533*, 2016.
 - [17] Jin Han Lee, Myung-Kyu Han, Dong Wook Ko, and Il Hong Suh. From big to small: Multi-scale local planar guidance for monocular depth estimation. *arXiv preprint arXiv:1907.10326*, 2019.
 - [18] Chenxu Luo, Zhenheng Yang, Peng Wang, Yang Wang, Wei Xu, Ram Nevatia, and Alan Yuille. Every pixel counts++: Joint learning of geometry and motion with 3d holistic understanding. *arXiv preprint arXiv:1810.06125*, 2018.
 - [19] Reza Mahjourian, Martin Wicke, and Anelia Angelova. Unsupervised learning of depth and ego-motion from monocular video using 3d geometric constraints. In *Proceedings of the IEEE Conference on Computer Vision and Pattern Recognition*, pages 5667–5675, 2018.
 - [20] Anh Nguyen, Jason Yosinski, and Jeff Clune. Deep neural networks are easily fooled: High confidence predictions for unrecognizable images. In *Proceedings of the IEEE conference on computer vision and pattern recognition*, pages 427–436, 2015.
 - [21] Adam Paszke, Sam Gross, Francisco Massa, Adam Lerer, James Bradbury, Gregory Chanan, Trevor Killeen, Zeming Lin, Natalia Gimelshein, Luca Antiga, et al. Pytorch: An imperative style, high-performance deep learning library. In *Advances in Neural Information Processing Systems*, pages 8024–8035, 2019.
 - [22] Anurag Ranjan, Joel Janai, Andreas Geiger, and Michael J Black. Attacking optical flow. In *Proceedings of the IEEE International Conference on Computer Vision*, pages 2404–2413, 2019.
 - [23] Mahmood Sharif, Sruti Bhagavatula, Lujo Bauer, and Michael K Reiter. Accessorize to a crime: Real and stealthy attacks on state-of-the-art face recognition. In *Proceedings of the 2016 acm sigsac conference on computer and communications security*, pages 1528–1540, 2016.
 - [24] Nathan Silberman, Derek Hoiem, Pushmeet Kohli, and Rob Fergus. Indoor segmentation and support inference from rgb-d images. In *European conference on computer vision*, pages 746–760. Springer, 2012.

- [25] Jiawei Su, Danilo Vasconcellos Vargas, and Kouichi Sakurai. One pixel attack for fooling deep neural networks. *IEEE Transactions on Evolutionary Computation*, 23(5):828–841, 2019.
- [26] Ilya Sutskever, James Martens, George Dahl, and Geoffrey Hinton. On the importance of initialization and momentum in deep learning. In *International conference on machine learning*, pages 1139–1147, 2013.
- [27] Christian Szegedy, Wojciech Zaremba, Ilya Sutskever, Joan Bruna, Dumitru Erhan, Ian Goodfellow, and Rob Fergus. Intriguing properties of neural networks. *arXiv preprint arXiv:1312.6199*, 2013.
- [28] Chaoyang Wang, José Miguel Buenaposada, Rui Zhu, and Simon Lucey. Learning depth from monocular videos using direct methods. In *Proceedings of the IEEE Conference on Computer Vision and Pattern Recognition*, pages 2022–2030, 2018.
- [29] Cihang Xie, Jianyu Wang, Zhishuai Zhang, Yuyin Zhou, Lingxi Xie, and Alan Yuille. Adversarial examples for semantic segmentation and object detection. In *Proceedings of the IEEE International Conference on Computer Vision*, pages 1369–1378, 2017.
- [30] Zhichao Yin and Jianping Shi. Geonet: Unsupervised learning of dense depth, optical flow and camera pose. In *Proceedings of the IEEE Conference on Computer Vision and Pattern Recognition*, pages 1983–1992, 2018.
- [31] Ziqi Zhang, Xinge Zhu, Yingwei Li, Xiangqun Chen, and Yao Guo. Adversarial attacks on monocular depth estimation. *arXiv preprint arXiv:2003.10315*, 2020.
- [32] Tinghui Zhou, Matthew Brown, Noah Snavely, and David G Lowe. Unsupervised learning of depth and ego-motion from video. In *CVPR*, volume 2, page 7, 2017.

Supplementary Material: Monocular Depth Estimators: Vulnerabilities and Attacks

1 White-box attack

1.1 Patch attack

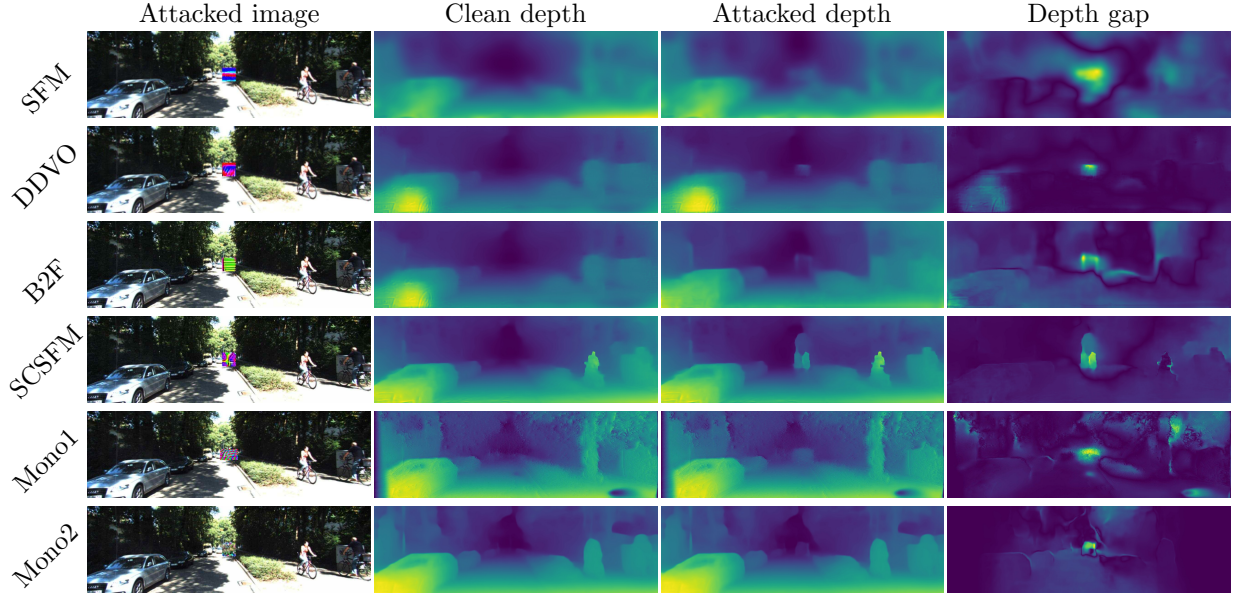


Figure 10: White-box patch test with sample of size 60×60 .

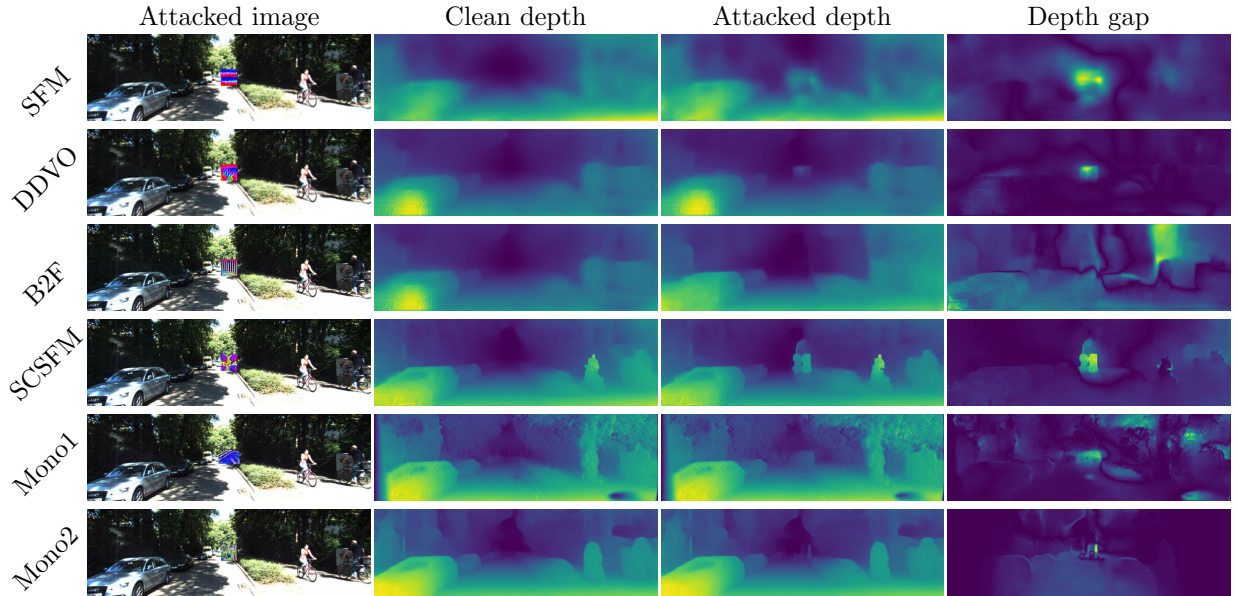


Figure 11: White-box patch test with patch size 72×72 .

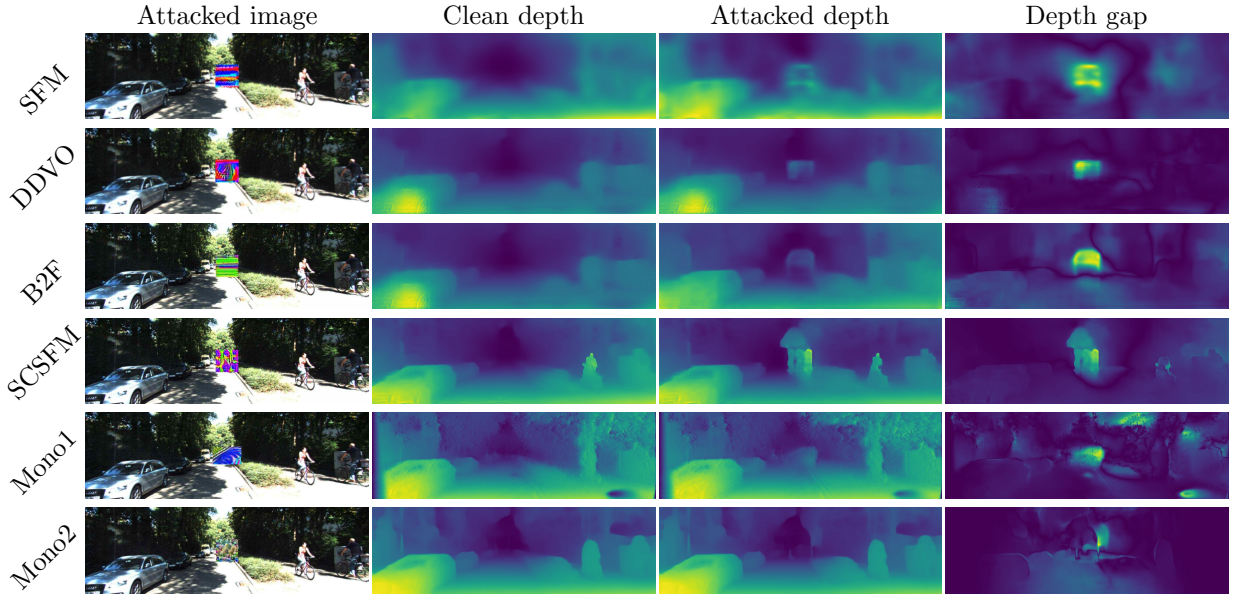


Figure 12: White-box patch test with patch size 100×100 .

Methods	Clean Absrel	Attacked							
		50×50		60×60		72×72		100×100	
		Absrel	Rel (%)	Absrel	Rel (%)	Absrel	Rel (%)	Absrel	Rel (%)
SFM [32]	0.1755	0.1887	8	0.2088	19	0.2193	25	0.2345	34
DDVO [28]	0.1488	0.1517	2	0.1519	3	0.1575	6	0.1712	16
B2F [14]	0.1358	0.153	13	0.1573	16	0.1573	16	0.1697	25
SCSFM [3]	0.1283	0.1533	20	0.1652	29	0.1759	38	0.2046	60
Mono1 [8]	0.1095	0.1166	7	0.1205	11	0.1271	17	0.1423	30
Mono2 [9]	0.1123	0.1239	11	0.1263	13	0.1317	18	0.1513	35

Table 5: White-box patch attack at different patch sizes.

1.2 Perturbation attack

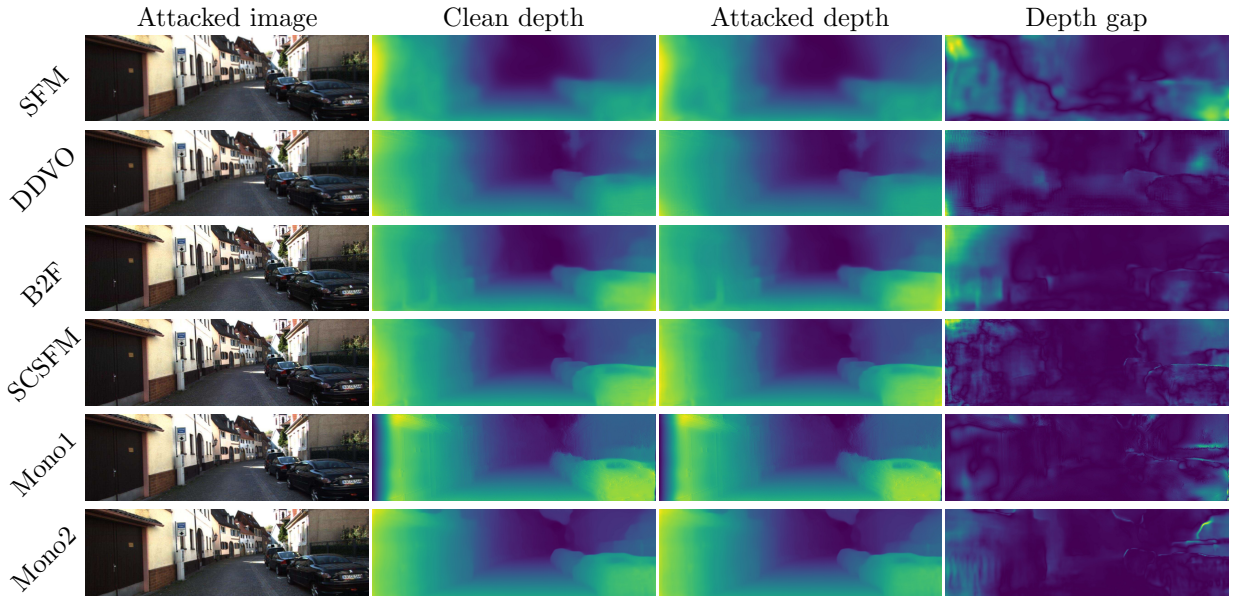


Figure 13: White-box perturbation test when $\eta = 0.01$

Methods	Clean	Attacked					
		$\eta = 0.01$		$\eta = 0.05$		$\eta = 0.1$	
		Absrel	Rel (%)	Absrel	Rel (%)	Absrel	Rel (%)
SFM [32]	0.1755	0.1955	12	0.4069	132	0.5913	237
DDVO [28]	0.1488	0.1568	6	0.7291	390	1.2197	720
B2F [14]	0.1358	0.1448	7	0.3725	175	0.4574	237
SCSFM [3]	0.1283	0.133	4	0.3389	165	0.4874	280
Mono1 [8]	0.1095	0.1115	2	0.2678	145	0.4341	297
Mono2 [9]	0.1123	0.1192	7	0.4037	260	0.4503	301

Table 6: Absolute Relative Error for white-box test on image specific perturbation attack.

Methods	Clean	Attacked					
		$\eta = 0.01$		$\eta = 0.05$		$\eta = 0.1$	
		RMSE	Rel (%)	RMSE	Rel (%)	RMSE	Rel (%)
SFM [32]	6.1711	6.6009	7	10.4535	70	12.3833	101
DDVO [28]	5.5072	5.7871	6	13.4231	144	18.662	239
B2F [14]	5.1615	5.4437	6	10.2015	98	12.2744	138
SCSFM [3]	5.2271	5.3731	3	9.35	79	12.5616	141
Mono1 [8]	5.1973	5.1973	0	8.8863	71	13.4931	160
Mono2 [9]	4.9099	5.0419	3	13.2947	171	14.7999	202

Table 7: RMSE for white-box test on image specific perturbation attack.

Methods	Clean	Attacked					
		$\eta = 0.01$		$\eta = 0.05$		$\eta = 0.1$	
		Absrel	Rel (%)	Absrel	Rel (%)	Absrel	Rel (%)
SFM [32]	0.1755	0.1783	2	0.2651	52	0.3975	127
DDVO [28]	0.1488	0.1526	3	0.5703	284	1.1942	703
B2F [14]	0.1358	0.1411	4	0.2213	63	0.3783	179
SCSFM [3]	0.1283	0.13	2	0.1834	43	0.3272	156
Mono1 [8]	0.1095	0.1102	1	0.1794	64	0.3659	235
Mono2 [9]	0.1123	0.1167	4	0.2826	152	0.3984	225

Table 8: Absolute Relative Error for white-box test on global perturbation attack.

Methods	Clean	Attacked					
		$\eta = 0.01$		$\eta = 0.05$		$\eta = 0.1$	
		Absrel	Rel (%)	Absrel	Rel (%)	Absrel	Rel (%)
SFM [32]	0.1755	0.1802	3	0.2023	16	0.2316	32
DDVO [28]	0.1488	0.1558	5	0.1763	19	0.1947	31
B2F [14]	0.1358	0.1491	10	0.1905	41	0.2158	59
SCSFM [3]	0.1283	0.1436	12	0.1707	34	0.1846	44
Mono1 [8]	0.1095	0.1175	8	0.1472	35	0.1711	57
Mono2 [9]	0.1123	0.133	19	0.1696	52	0.2052	83

Table 9: Absolute relative error of white-box FGSM attack.

Methods	Clean	Attacked					
		$\eta = 0.01$		$\eta = 0.05$		$\eta = 0.1$	
		RMSE	Rel (%)	RMSE	Rel (%)	RMSE	Rel (%)
SFM [32]	6.1711	6.2857	2	6.8239	11	7.4746	22
DDVO [28]	5.5072	5.7242	4	6.2509	14	6.6626	21
B2F [14]	5.1615	5.349	4	5.9803	16	6.4383	25
SCSFM [3]	5.2271	5.3107	2	5.5715	7	5.9258	14
Mono1 [8]	5.1973	5.347	3	5.9713	15	6.5298	26
Mono2 [9]	4.9099	5.4985	12	6.1803	26	6.891	41

Table 10: RMSE of white-box FGSM attack.

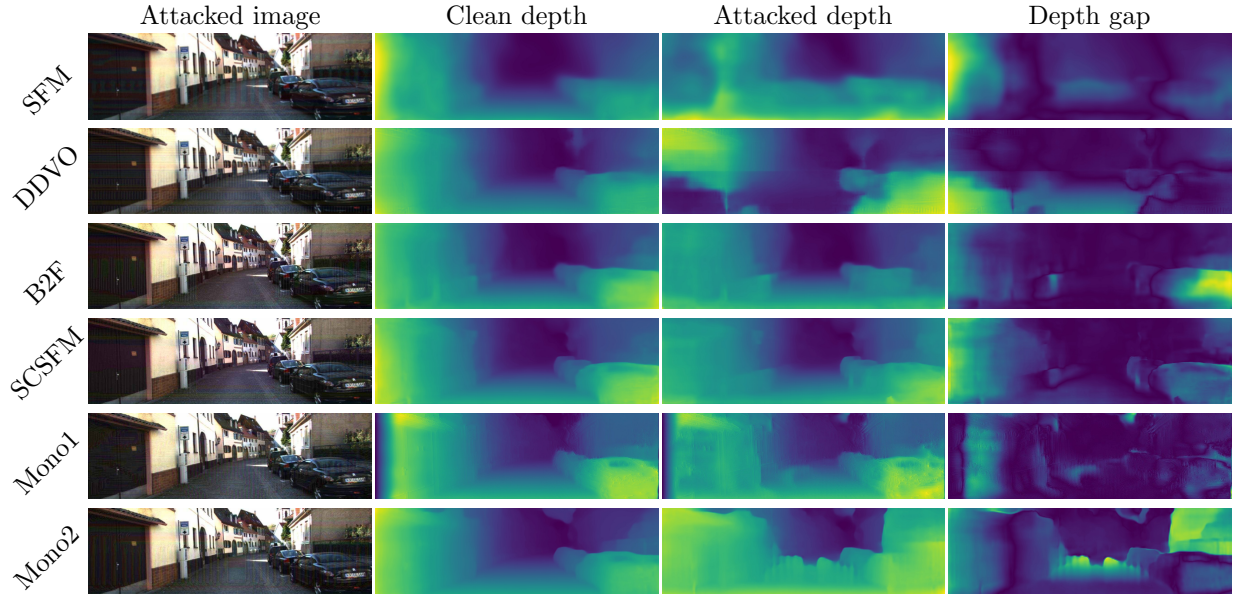


Figure 14: White-box perturbation test when $\eta = 0.05$.

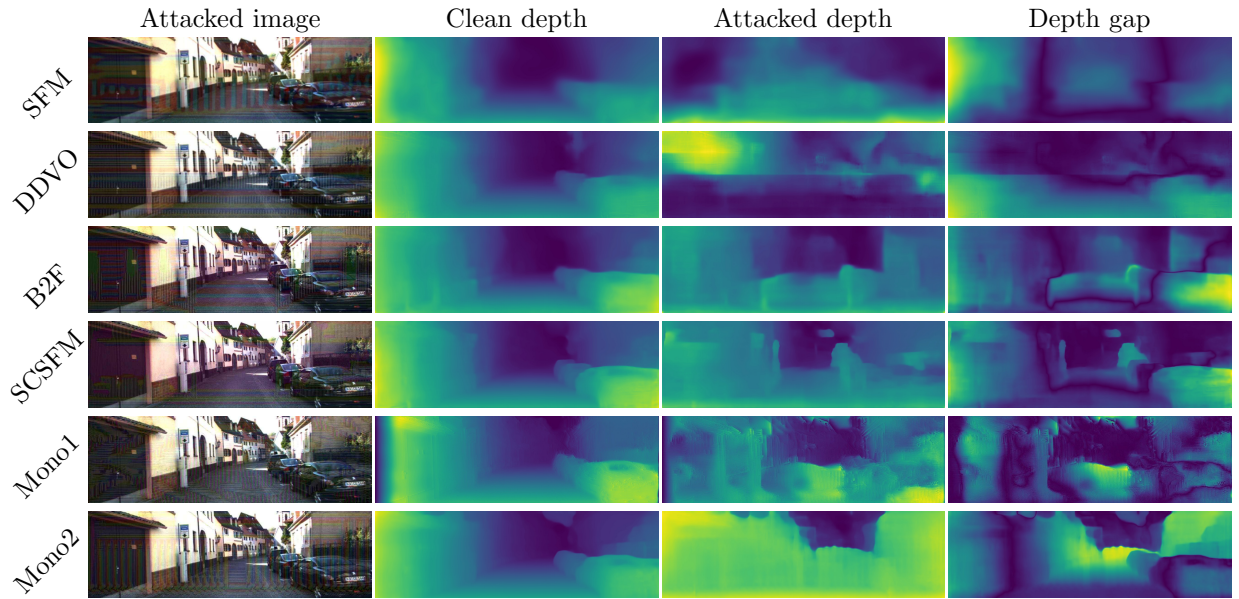


Figure 15: White-box perturbation test when $\eta = 0.1$

2 Black-box attack

Methods	Clean Absrel	Patch									
		SFM [32]		DDVO [28]		SCSFM [3]		Mono1 [8]		Mono2 [9]	
		Absrel	Rel (%)	Absrel	Rel (%)	Absrel	Rel (%)	Absrel	Rel (%)	Absrel	Rel (%)
SFM [32]	0.1755	-	-	0.1962	12	0.1858	6	0.191	9	0.1803	3
DDVO [28]	0.1488	0.1488	0	-	-	0.1514	2	0.1496	1	0.1577	6
B2F [14]	0.1358	0.1422	5	0.1425	5	0.1432	6	0.1401	4	0.1444	7
SCSFM [3]	0.1283	0.1448	13	0.1477	16	-	-	0.1462	14	0.1343	5
Mono1 [8]	0.1095	0.1265	16	0.12	10	0.119	9	-	-	0.115	6
Mono2 [9]	0.1123	0.1136	2	0.116	4	0.1189	6	0.1146	3	-	-

Table 11: Black-box patch attack with patch size 72×72 .

Methods	Perturbation											
	SFM [32]		DDVO [28]		B2F [14]		SCSFM [3]		Mono1 [8]		Mono2 [9]	
	Absrel	Rel (%)	Absrel	Rel (%)	Absrel	Rel (%)	Absrel	Rel (%)	Absrel	Rel (%)	Absrel	Rel (%)
SFM [32]	-	-	0.1842	5	0.181	4	0.1775	2	0.1775	2	0.1859	6
DDVO [28]	0.1799	21	-	-	0.1675	13	0.1534	4	0.1598	8	0.1667	13
B2F [14]	0.1675	24	0.5703	284	-	-	0.1724	27	0.1553	15	0.1643	21
SCSFM [3]	0.1512	18	0.161	26	0.165	29	-	-	0.1413	11	0.1565	22
Mono1 [8]	0.1147	5	0.124	14	0.1242	14	0.1255	15	-	-	0.1228	13
Mono2 [9]	0.1401	25	0.1452	30	0.1454	30	0.1519	36	0.129	15	-	-

Table 12: Black-box perturbation attack when $\eta = 0.05$

3 Feature visualization

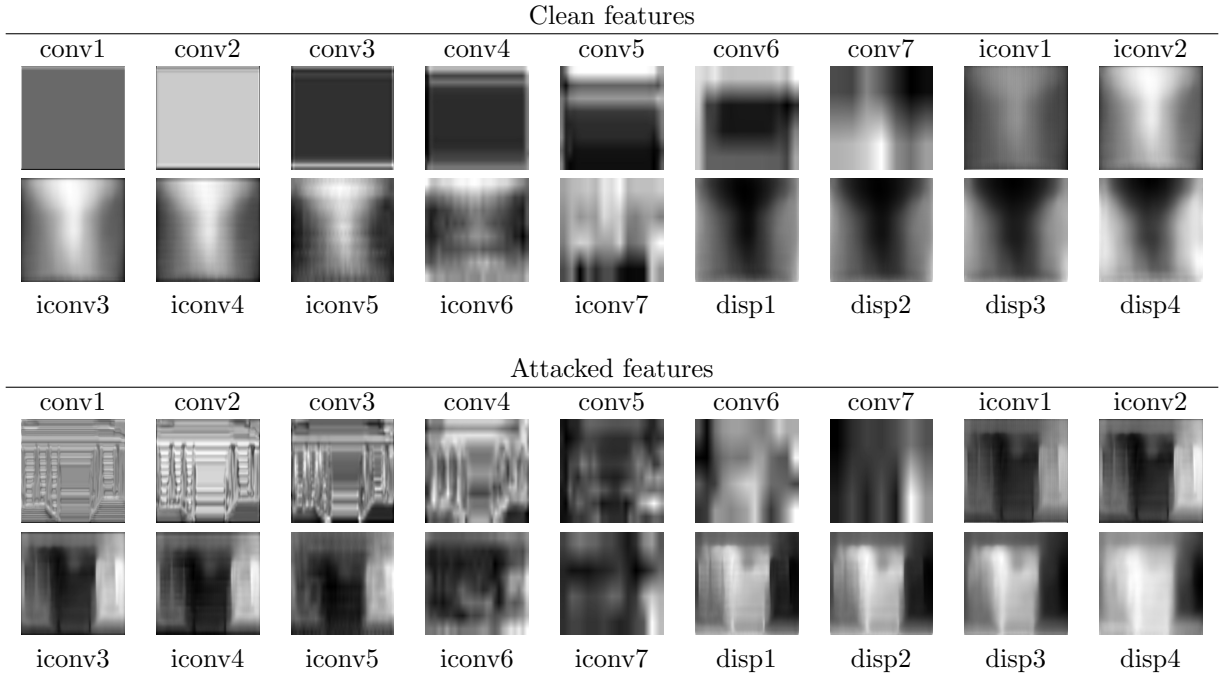


Figure 16: Layer-wise B2F [14] feature visualization. ‘convx’ are encoder layers and ‘iconvx’ are decoder layers.